# Quantifying and modulating protein encapsulation in guanosine-based supramolecular particles

Luis A. Prieto-Costas, Génesis R. Rivera-Cordero & José M. Rivera*

Department of Chemistry and Molecular Sciences Research Center, University of Puerto Rico at Río Piedras, San Juan, PR, 00926. E-mail: jose.rivera151@upr.edu

## ABSTRACT

The encapsulation of proteins is an effective way to preserve their structure and enhance their function. One exciting possibility is adjusting the protective agent to match the specific protein's characteristics to influence its properties. In a recent study, we developed a flow cytometry-based method to quantify the encapsulation of small molecule dyes in colloidal particles made from guanosine derivatives (SHS particles). We aimed to determine if this method could quantify protein encapsulation and track changes and if proteins could be tuned to bind to these particles. Our results showed that FITC-labeled proteins had apparent association constants in the micromolar range, with hydrophobicity as the dominant factor enhancing the affinities. Confocal laser scanning microscopy imaging supported these results and provided additional information about protein distribution within the particles. We also tested the feasibility of tuning avidin affinity (AVI) for SHS particles with a biotin ligand. We found that increasing the amount of biotin initially enhanced AVI binding, but then reached saturation, which we hypothesize results from non-covalent cross-linking caused by strong biotin/AVI interactions. CLSM images showed that the linker also impacted AVI distribution within the particles. Our strategy provides an advantage over other methods for quantifying protein encapsulation by being suitable for high-throughput analysis with high reproducibility. We anticipate that future efforts of using lower affinity ligands would result in better strategies for modulating protein affinity for drug-delivery applications.

## 1. INTRODUCTION

Nanotechnology has made a significant impact on various fields, including affinity-based separations, sensor development, and the development of new therapeutics. One promising area for nanotechnology is in the encapsulation and transportation of small-molecule therapeutics with low solubility in an aqueous environment using drug delivery systems. [1] Hydrophilic therapeutics, such as biomacromolecules, present additional challenges that can be addressed using these systems. Encapsulation of proteins in particles can provide protection against degradation and loss of biological function. [2–4] However, existing methods for encapsulation often denature proteins due to harsh conditions or changes in protein structure caused by covalent modifications. [5,6] To overcome these challenges, encapsulation methods that rely on the natural affinity of proteins towards a given particle in an aqueous environment represent an attractive strategy.

One way to deliver drugs to a specific target is to use affinity-based systems that can trap the drug molecules inside a carrier without exposing them to harsh conditions. [7] These systems rely on the natural attraction between molecules such as proteins, which are held together by weak forces (e.g., H-bonds, electrostatic, van der Waals).[8] By adjusting these forces, it is possible to achieve precise control over how the drug is encapsulated and released.[9] However, to do this effectively, it is important to understand how the carrier interacts with the drug at a fundamental level. For this purpose, we have developed a method based on Flow cytometry (FC), which can measure the relative affinity of colloidal particles made of guanosine.

We have developed guanosine-based particles that consist of self-assembled 2'-deoxyguanosine derivatives (G-derivatives). These derivatives form supramolecular G-quadruples (SGQs) when $K^+$ ions are present. By increasing the temperature, we can further assemble the SGQs into Supramolecular Hackly Sacks (SHS) or SHS particles.[10,11] These particles can encapsulate various small and large molecules through non-covalent interactions.[12,13] We have demonstrated that our particles have promising properties for various applications in biotechnology and nanomedicine.[14,15] However, we still face some challenges in understanding and manipulating the

interactions between these particles and different macromolecules. For example, we need to investigate how the size, shape, charge, and surface chemistry of the particles affect their binding affinity to proteins, DNA and other biomolecules. To further the potential of these particles for multiple applications, we still need to study how different macromolecules interact with our system and how we can control their relative binding affinity. We also need to explore how we can modulate this relative binding affinity by changing the environmental conditions or introducing external stimuli. By addressing these questions, we can optimize our system for specific purposes and enhance its functionality and versatility.

The aim of this study is to measure the relative affinities of proteins for two kinds of SHS particles using a novel FC-based method recently developed by our group.[16] We also want to examine if we can change the relative binding strength of a protein by adding an affinity ligand (Figure 1). These findings enhance our comprehension of how to measure and control the interactions between proteins and the colloidal SHS particle family, laying the groundwork for their expanded utility, such as in the precise release of therapeutic agents. It's worth noting that the exploration of controlled release studies falls beyond the scope of this investigation.

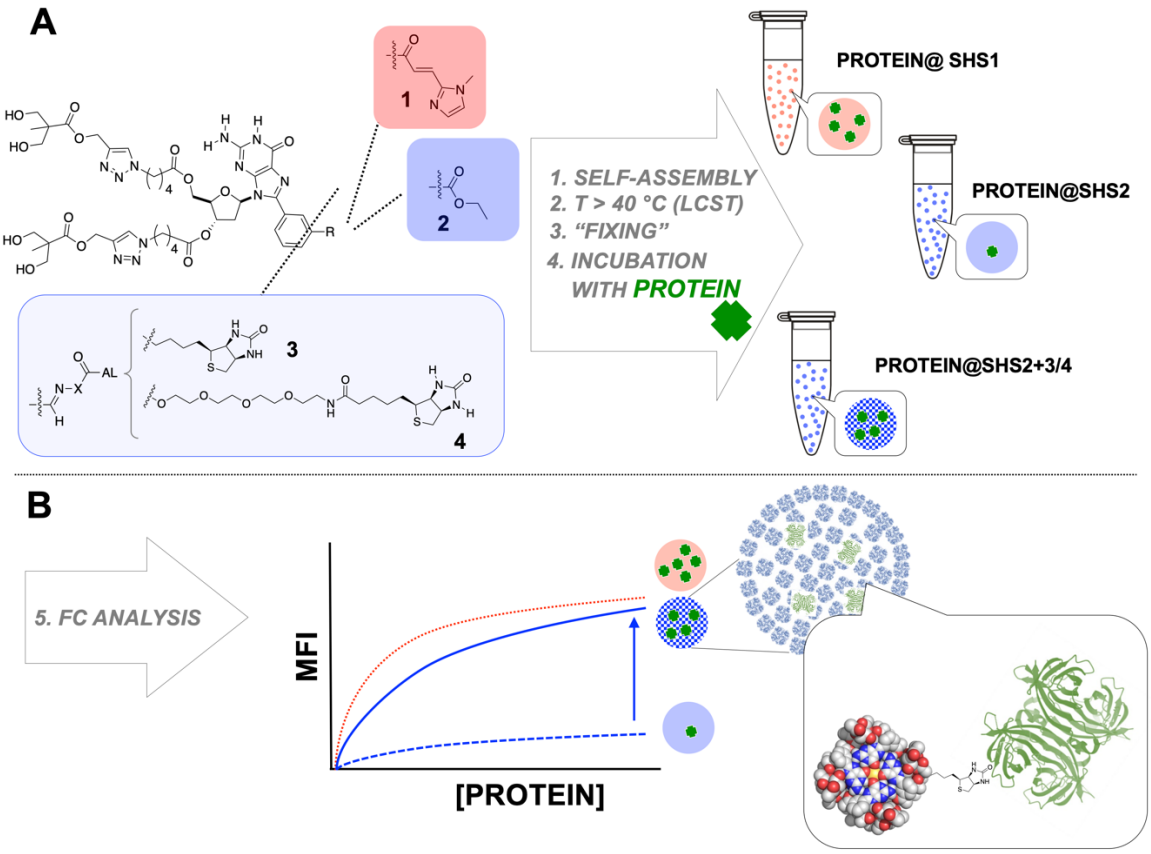


**Figure 1.** Experimental overview of the methodology of the encapsulation of proteins in SHS particles. (A) G-derivatives self-assembled in the presence of a cation to form supramolecular G-quadruplexes (1). The self-assembled structures are further assembled by an increase in temperature to form supramolecular Hacky Sacks (SHS) particles (2). The temperature to promote the formation of the SHS particles in this study was 40 °C. The SHS particles are kinetically stabilized (or "fixed") by lowering the ionic strength of the solution (3). All the encapsulations in this study were done using fixed SHS particles. Protein incubation with SHS particles was done for 1 h at 40 °C (4). (B) After incubation the **Protein@SHS** complex was further studied with various techniques like flow cytometry and confocal microscopy (5). Adapted with permission from ref. 16 (Prieto-Costas 2021) copyright 2021 American Chemical Society.

This study investigates how FITC-labeled proteins bind to SHS particles with different molecular descriptors. We measured apparent affinity constants of various proteins for SHS particles using fluorescence spectroscopy (see Figure S1 for a graphical depiction of all the proteins studied). We also explored how biotinylated G-derivatives affect the binding of Avidin to SHS particles. Our results provide insights into the molecular interactions between SHS particles and proteins.

## 2. EXPERIMENTAL

### *2.1 Synthesis of G-derivatives*

The synthesis of **1**, **2** and **5** were performed as published elsewhere.[11,17,18] Column chromatography was done using silica gel 60, 0.04-0.063 mm, and TLC was performed using EMD silica gel 60 F254 glass backed plates from Sorbent Technologies. Visualization of spots was affected using UV light.

### *2.2 NMR measurements*

1D/2D NMR spectra was recorded on Bruker AV-500 (TopSpin v2.0) equipped with 5 mm BBO probe and nominal frequencies of 500.13 MHz for proton or 125.77 MHz for carbon, respectively. The solvents used in these experiments were deuterated DMSO (DMSO-$d_6$) or deuterated chloroform ($CDCl_3$). $^{1}H$ and $^{13}C$ NMR chemical shifts were reported in parts per million (ppm) relative to the traces of non-deuterated solvent as an internal reference. The following abbreviations were used to describe the peak multiplicities: s, singlet; d, doublet; t, triplet; m, multiplet, or a combination of these.

### *2.3 Dynamic Light Scattering and Zeta Potential measurements*

A Zetasizer Nano ZS (model ZEN3600) from Malvern Panalytical with a 4-mW laser of 632.8 nm wavelength and a backscatter angle of 173° and a low-volume quartz batch cuvette (ZEN2112) was used to measure the hydrodynamic diameter of all SHS particles at 25 °C. For Zeta-potential measurements a Malvern Panalytical disposable capillary cell (DTS1070) was used. All the measurements were performed following the incubation procedure. The instrument data was collected and exported using the Zetasizer software, version 7.10; Malvern Panalytical Ltd, United Kingdom, 2014 and imported into Microsoft Excel to construct the DLS plots.

### *2.4 Flow Cytometry measurements*

Flow cytometry measurements were made using a BD Acurri$^{TM}$ C6 Flow Cytometer from BD Sciences with standard laser configurations (488 nm and 640 nm) and detectors (FL1

525/25, FL2 585/15, FL3 670 LP and FL4 675/25). Confocal microscopy images were obtained in a Nikon Eclipse Ti-E Inverted Microscope with an emission range of (400–730) nm. The objective used for all the samples was Plan Apo Alpha 100*X* with oil.

Eppendorf tubes containing the **Protein@SHS** complex samples were vortexed before they were introduced to the sample injector port of the flow cytometer. This process was repeated for each protein concentration. For each protein a forward scatter versus side scatter density plot (FCS vs SSC) was used to create a gate for the SHS control, which was subsequently used for all concentrations. At least 10K events were recorded for each experiment. Histograms were generated from each gated density plot. The change in median fluorescence intensity of each sample was plotted as a function of concentration to generate binding isotherms. All the reported **Protein@SHS** complexes were excited with a 488 nm laser and the fluorescence detector used was FL1.

The apparent dissociation constant ($K_D$) was obtained GraphPad Prism version 6.00 for Mac OS X, GraphPad Software, La Jolla California USA. Hyperbolic curve fitting, or one-site specific binding equation [$y = B_{max}*X/(K_D + X)$], was used to calculate $K_D$. $K_D$ is defined as the concentration of dye needed to achieve a half-maximum binding at equilibrium. The apparent association constants ($K_A$) were calculated using the reciprocal of $K_D$.

*2.5 Protein labeling protocol*

For protein labeling and bioconjugation reactions we used a modification of the protocol recommended by the manufacturer (Millipore-Sigma). Briefly, a 2 mg/mL pure protein sample was dissolved in 0.1 M sodium carbonate buffer, pH 9. The labeling agent fluorescein isothiocyanate (FITC) was used at 1 mg/mL in anhydrous DMSO. In the 4 °C freezer, for each 1 mL of protein sample, we slowly added 50 µL of FITC reagent in 5-6 µL aliquots. The reaction was left stirring for 8 h in the dark. Once the reaction was completed, we proceeded to purify the protein by removing the excess FITC using Size-Exclusion Chromatography Columns (PD10 column) with 1X PBS, pH 7.4 as the eluent. The resulting pure protein was concentrated using AMICON filter tubes (10 kDa or 30 kDa MWCO) via centrifugation (at 3K rpm for 2 h) after which we measured the concentration via UV-VIS spectroscopy.

*2.6 Preparation of the SHS and Protein@SHS complexes*

Solutions of **1** and **2** were prepared by dissolving 3.2 mg of **1** and 3.1 mg of **2** in 0.650 mL of PBS from Fisher Scientific (pH 7.4) to yield a final monomer concentration of 5 mM. To these solutions, 50.5 mg of potassium thiocyanate (KSCN) was added to achieve a final concentration of 800 mM. The samples were sonicated for ~1 min and left equilibrating in the refrigerator (-10 °C) overnight. These samples are termed SGQ solutions. SHS solutions form upon heating the SGQ solution in a water bath at 40 ºC. The preparation of heteromeric assemblies is described in the self-assembly section.

A solution containing 5 mM **SHS1** or **SHS2** and 800 mM KSCN in 1X PBS was made fresh and left in the freezer for 1 day. Solutions of 0.3 mM $f$-SHS, 50mM KSCN were prepared by diluting 138 µL of SHS solution in 2.162 mL of PBS at 40 °C. Then, 100 µL of these solutions were added into 21 microtubes organized in 7 rows containing 3 tubes each. These tubes correspond to the triplicate samples of 0, 1, 5, 10, 20, 40 and 80 µM protein concentration. Using a previously made protein solution we made serial dilutions to prepare 1600, 800, 400, 200, 100 and 20 µM. To achieve this, we used the protein to stock and diluted it to 1600 µM. Each subsequent dilution was prepared by taking a 50 µL aliquot and then adding an additional 50 µL of 1X PBS. From these solutions we extracted 5 µL aliquots into the corresponding tube of the 21 microtubes containing 100 µL of SHS. This resulted in triplicate samples containing 0, 1, 5, 10, 20, 40 and 80 µM protein concentrations with constant concentrations of salt and SHS particles. These samples were then left to incubate at 100 rpm, 40 °C for 1 h before the subsequent with flow cytometry measurements.

*2.7 Confocal Laser Scanning Microscopy*

Confocal microscopy images were obtained in a Nikon Eclipse Ti-E Inverted Microscope with an emission range of (400–730) nm. The objective used for all the samples was a Plan Apo Alpha 100*X* with oil. After the incubation process, 10 µL of **Protein@*f*-SHS** from each sample were added to the microscope slide and covered with a glass cover

slip. Two microscope slides were prepared for each sample (n = 2). Two images per slide were taken one day after preparation. All samples were excited with the 488 nm laser. The enrichment index was calculated by dividing the fluorescence intensity inside the particle ($FI_{ins}$) by the fluorescence of the surrounding medium ($FI_{inside}/FI_{outside}$).

*2.8 Molecular modeling studies*

Molecular models were constructed and minimized using: OPLS_2005 *(MacroModel)*, Version Maestro 9.3.5; Schrödinger, LLC: New York, 2007, with water as a continuum solvent. This SGQ model was published previously.[19] (García-Arriaga, 2016). All structures were minimized with restraints on the $K^+$ ions and the G-tetrad core up to the C1' of the sugar, allowing free movement of the side chains.

## 3. RESULTS AND DISCUSSION

*ever3.1 Preparation of SHS and the Protein@SHS complexes*

The SHS particles are prepared through the self-assembly of G-derivatives **1** and **2**, which vary in the substitution at the C8 of the guanine moiety, into supramolecular G-quadruplexes (SGQs) with the help of potassium thiocyanate (Figure 1). [20,21] The SHS particles, designated as **SHS1** and **SHS2**, respectively, are then formed through further thermally induced self-assembly, taking advantage of the LCST phenomenon (please refer to the experimental section for more information).The SHS particles are prepared through the self-assembly of G-derivatives **1** and **2**, which vary in the substitution at the C8 of the guanine moiety, into supramolecular G-quadruplexes (SGQs) with the help of potassium thiocyanate (Figure 1). [19,20] The SHS particles, designated as **SHS1** and **SHS2**, respectively, are then formed through further thermally induced self-assembly, taking advantage of the LCST phenomenon (please refer to the experimental section for more information).

The SHS particles produced have an average hydrodynamic diameter greater than 1 µm, making them ideal for FC studies, with **SHS1** measuring at 3.2 µm and **SHS2** at 2.6

μm (Figure S2; Table S1). Both particles possess negative zeta potentials, with **SHS1** at -5.6 mV and **SHS2** at -9.0 mV, consistent with our previous reports.[13] From this information, we can infer those cationic proteins, which have high pI values, are expected to have a greater affinity towards these SHS particles.

To encapsulate the protein, it was titrated into a fixed amount of SHS particle, forming a complex (**PROT@SHS#**, where PROT represents the protein abbreviation and # represents the G-derivative **1** or **2** identifier).[22,21] The FC-based method, as recently described by us,[16] was used to determine the apparent affinity of proteins towards the SHS particles. To create fluorescent particles for this method, commercially available proteins were labeled with fluorescein isothiocyanate (FITC), as described in the experimental section. Subsequent measurements of the median fluorescence intensity (MFI) by FC were used to generate saturation graphs that allowed the calculation of $K_A$ values (using GraphPad software), as explained in the following section.

For this study, we selected globular proteins with varying physical characteristics such as cationic or anionic properties, different isoelectric points (pI), and a wide range of molecular weights (MW) (Figure S1). Our focus is to evaluate how parameters like pI, aliphatic index, MW, and average hydropathy (GRAVY) of these proteins affect their apparent affinity towards SHS particles.

*3.2 Flow cytometry studies*

Following the measurement of SHS complexes by the FC instrument, we conducted the primary analysis using density plots and histograms. Density plots were generated from the light scattering of the laser, with at least 10K events analyzed for particle size (forwards scatter or FCS) and granularity or internal complexity (side scatter or SSC).[23] The resulting histograms allowed for the visualization of the population of fluorescent particles and/or the number of particles that encapsulated the fluorescent proteins (Figure S3-S20).Following the measurement of SHS complexes by the FC instrument, we conducted the primary analysis using density plots and histograms. Density plots were generated from the light scattering of the laser, with at least 10K events analyzed

for particle size (forwards scatter or FCS) and granularity or internal complexity (side scatter or SSC).[22] The resulting histograms allowed for the visualization of the population of fluorescent particles and/or the number of particles that encapsulated the fluorescent proteins (Figure S3-S20).

*3.3 Density plots and histograms*

By analyzing density plots and histograms, we were able to identify qualitative trends on how the populations of SHS particles change after interacting with a given protein. For instance, while the density plots of **PEP@SHS1** showed no significant changes in their average size or morphology (Figure S17), the related **PEP@SHS2** revealed a noticeable shift in population at high protein concentrations (Figure S18). This shift could be attributed to changes in particle size and/or its internal structure. Our hypothesis was that the changes in size upon encapsulation might be due to electrostatic repulsion between the SHS particles and **PEP**, considering its negative ZP and the lowest pI (anionic at pH 7.4) relative to all the other proteins studied.

*3.4 Binding isotherms (saturation curves)*

After measuring the **PROT@SHS** complexes using FC, binding isotherms were generated by plotting MFI against concentration (Figure 2). The saturation of the **PROT@SHS2** complexes is generally higher than that of the corresponding **PROT@SHS1**, primarily due to differences in the dye/protein ratio (Table S2). For instance, **TRY** has the highest dye/protein ratio, which explains its high saturation MFI (Table S1). Therefore, evaluating and comparing the apparent affinities of different proteins towards a given particle based solely on binding isotherms (Figure 2) or CLSM images (Figure 4) can be misleading. However, such comparisons can provide qualitative information when evaluating a given labeled protein towards a different particle. In this study, **SHS2** has slightly higher affinity towards most proteins, but the greater negative ZP of this particle is unlikely to be the main parameter dictating the apparent affinity of proteins towards SHS particles since both cationic and anionic proteins show high affinities.

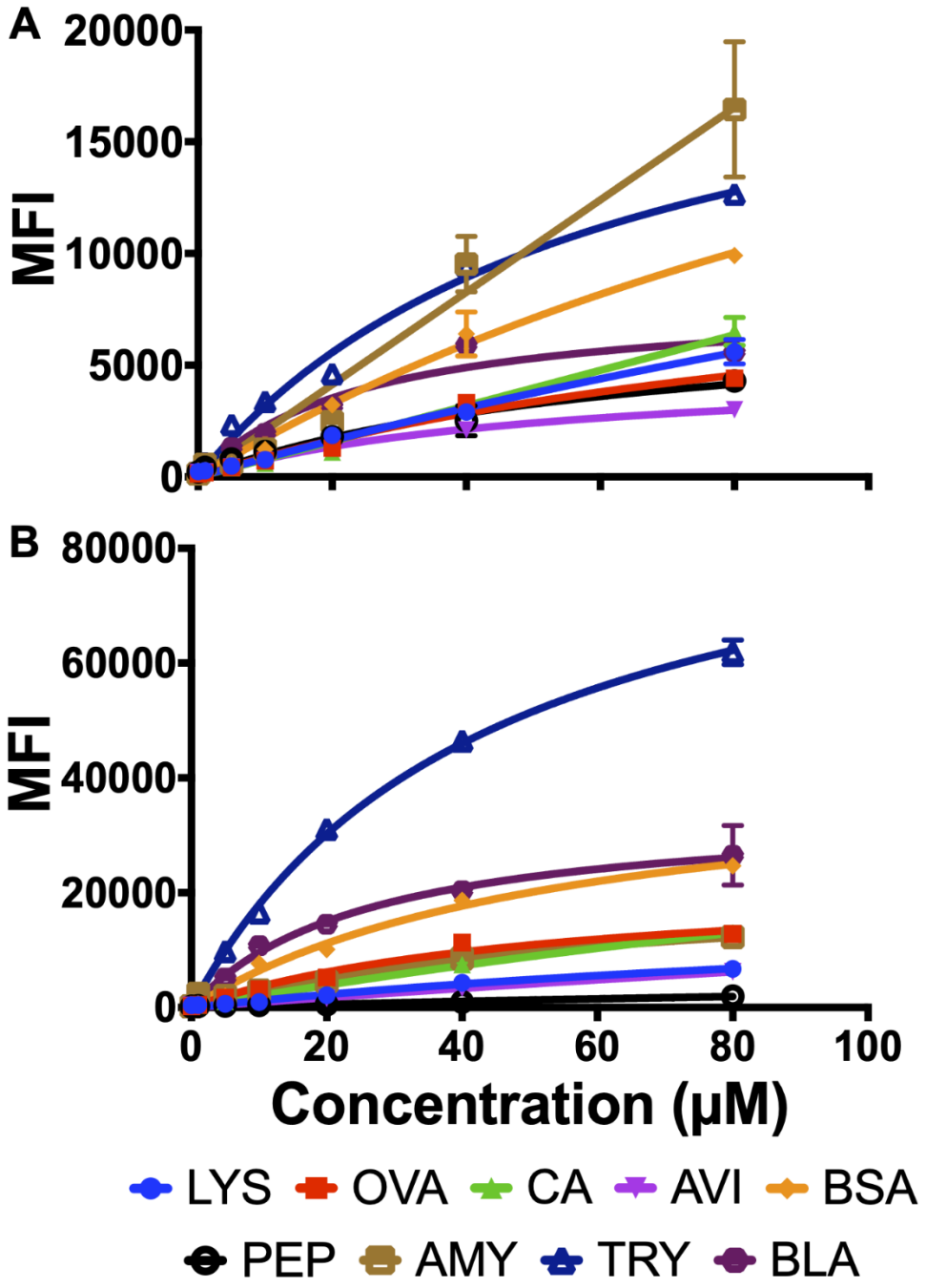


**Figure 2.** Binding isotherms for the encapsulation of FITC-labeled proteins in (A) **SHS1** and (B) **SHS2**. Error bars represent the standard deviation of triplicate measurements. **SHS**: 299 μM of **1** and **2**, 52 mM KSCN, PBS pH 7.4. Encapsulation concentration of the proteins: 0, 1, 5, 10, 20, 40 and 80 μM.

*3.5 $K_A$ bar graphs and correlation plots*

The binding isotherms were fitted to calculate the apparent dissociation constants ($K_D$), which were then used to calculate the corresponding apparent association constants ($K_A$) (Figure 3, Table S3).

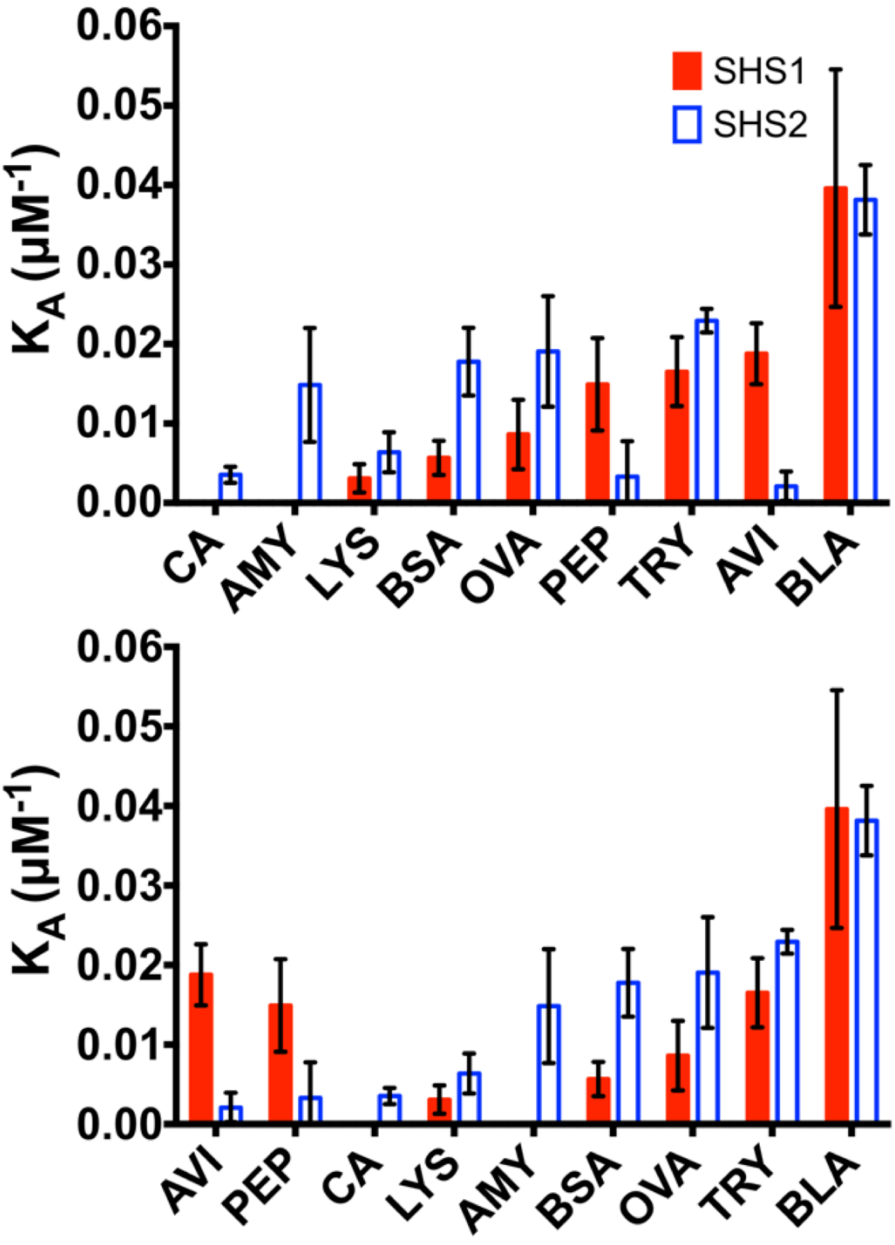


**Figure 3.** Apparent association constants ($K_A$) of FITC-labeled proteins towards **SHS1** and **SHS2** determined from FC measurements. Plots A and B contain the same $K_A$ values, but they are arranged in ascending order for (A) **SHS1** and (B) **SHS2**. Error bars represent the standard deviation of the measurement reported by PRISM GraphPad.

In a recent report,[16] we observed that the SHS prefer cationic dyes, which showed higher affinities than their anionic counterparts. Based on this finding, we hypothesized that a similar trend would hold for the proteins studied in this research. However, the correlation plots between apparent affinity constants and pI showed that charge complementarity did not dominate the interactions between proteins and SHS particles (Figure S30). Surprisingly, the SHS particles seem to provide a relatively unbiased scaffold for binding proteins. For example, **BLA** and **TRY**, which have opposite electrostatic characters as cationic and anionic proteins respectively, showed the highest apparent affinity for both particles. This observation led us to prepare correlation graphs with a range of molecular descriptors to further investigate the possible molecular origin of this behavior.

Our group's previous studies have suggested a possible inverse relationship between molecular weight and apparent affinity towards SHS particles for both proteins and polysaccharides.[13] However, for the proteins investigated in this study, the relationship between apparent affinity and molecular weight only shows a slight trend (FigureS31). For instance, the lower molecular weight protein, **BLA**, consistently displays high apparent affinities for both particles. Conversely, **LYS**, which is slightly lighter, exhibits one of the lowest apparent affinities of all the proteins tested. Another noteworthy finding is the apparent inversion of affinity between **AVI** and **BSA**. Specifically, **AVI** shows higher values, while **BSA** shows lower values for **SHS1**, but this trend reverses for **SHS2**. These findings demonstrate that apparent affinities of any given protein for SHS particles depend on a complex interplay of multiple parameters.

As the constituent G-derivatives of the SHS particles are amphiphilic molecules11, we hypothesized that hydrophobicity would play a crucial role in protein encapsulation. To test this hypothesis, we analyzed the correlation between two parameters used to quantify the lipophilicity (aliphatic index; Figure S32) and hydrophobicity (GRAVY parameter; Figure S33) of proteins. The former is defined as the relative volume occupied by the lipophilic side chains in each protein, while the latter indicates greater

hydrophobicity for positive values. Both parameters suggest slightly higher apparent affinities for more lipophilic/hydrophobic proteins, although the correlation is also weak.

Compared to the proteins evaluated in this study, the apparent affinities for small molecule dyes, as determined by the same FC method,[16] are significantly higher. Specifically, small molecule dyes exhibit greater average affinities for **SHS1** and **SHS2** by a factor of 5 and 11, respectively. No SHS particle displays higher apparent affinities for all types of molecules. Moreover, the average apparent affinities of small molecule dyes for **SHS2** are 1.6 times greater than those for **SHS1**. However, with proteins, **SHS1** particles exhibit slightly higher apparent affinity (by a factor of 1.4) than **SHS2** (See SI for details). These results demonstrate the potential of this FC method to rapidly screen a wide range of molecules and obtain relative affinities for biologically significant molecules. At this stage, we aimed to compare these trends with another crucial tool in cell biology, Confocal Laser Scanning Microscopy (CLSM).

*3.6 Confocal laser scanning microscopy studies*

To enhance our understanding of this system, we employed Confocal Laser Scanning Microscopy (CLSM) as a supplementary technique to FC (Figure 4). This technique is commonly used to measure the encapsulation of cargo in particles. CLSM provides qualitative information that is crucial for comprehending not only the apparent affinity for a specific guest molecule but also its corresponding spatial distribution within the particle. The former can be quantified as an enrichment index (EI),[24] which represents the partition ratio of the protein inside and outside the particle, as determined by the CLSM-acquired images (Figure 5).The former can be quantified as an enrichment index (EI),[23] which represents the partition ratio of the protein inside and outside the particle, as determined by the CLSM-acquired images (Figure 5).

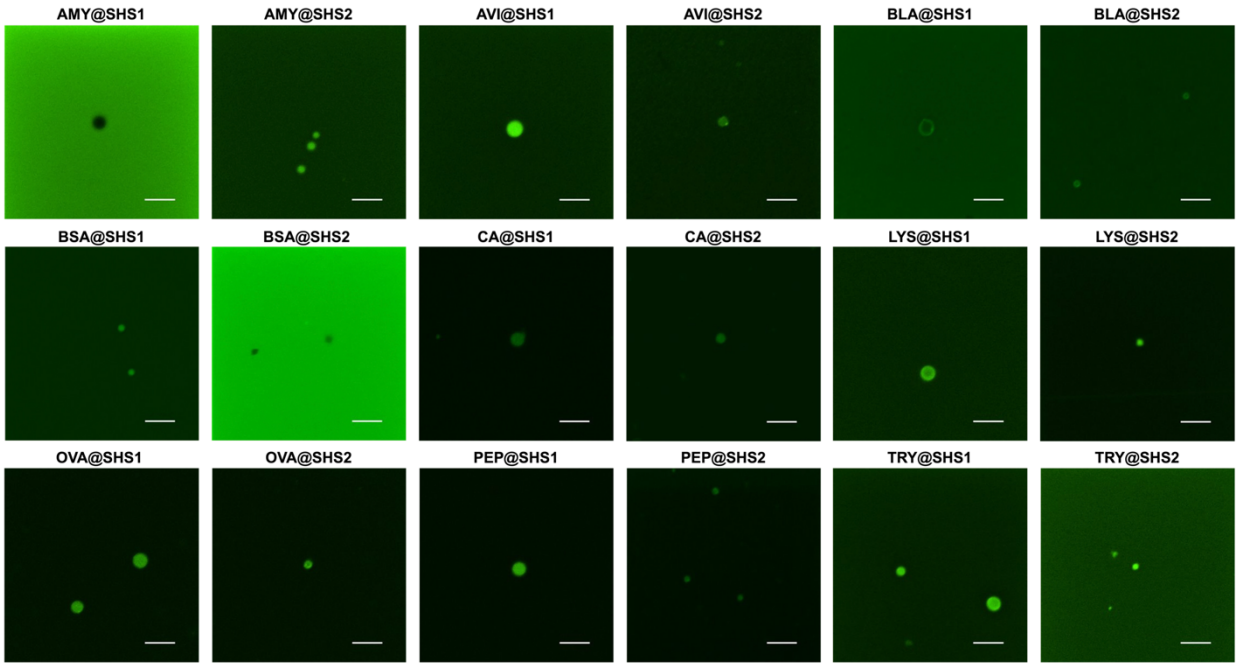


**Figure 4.** Confocal microscopy images for FITC-labeled proteins encapsulated in **SHS1** and **SHS2**. The concentration of the proteins in each sample was 80 μM and for **SHS1** and **SHS2** was 299 μM of G-derivatives **1** or **2**, in 52 mM KSCN, PBS pH 7.4. The excitation laser used was 488 nm and all scale bars = 5 μm.

Due to the relatively low affinities of the SHS particles for the proteins evaluated in this study, the CLSM images of the Protein@SHS complexes were obtained after incubating the particles with the highest concentration used in the FC experiments (80 μM). The images indicate that, except for **AMY** and **BSA**, which are excluded from **SHS1** and **SHS2**, respectively, all other proteins are encapsulated to varying degrees. Another interesting observation from the CLSM images is that the complexes between **SHS1** and **BLA** and to a lesser degree, **LYS**, show a protein encapsulation with a preferential distribution on the periphery of the particles (peripheral encapsulation). **AMY** and **BSA** are anionic proteins of high molecular weight, and their apparent exclusion from the SHS particles is consistent with the low apparent affinity constants determined using FC measurements. The enrichment index provides an independent quantitative measurement of the effective internalization of the proteins, as well as information about the distribution and other morphological features of the particles. However, it is important to keep in mind that FC provides a view of the entire population of particles,

while confocal microscopy, and thus, enrichment index, only captures a snapshot of a small segment of that population.[25] The enrichment index is susceptible to a relatively large variability due to the limited number particles included in its calculation (in our case an average of 6 particles per image; Figure 4, Table S4). [24] The enrichment index is susceptible to a relatively large variability due to the limited number particles included in its calculation (in our case an average of 6 particles per image; Figure 4, Table S4). With flow cytometry this limitation is overcome due to the significantly larger population size (10,000 particles or counts). Therefore, it is not surprising that the apparent affinities obtained using both techniques may differ in some cases.

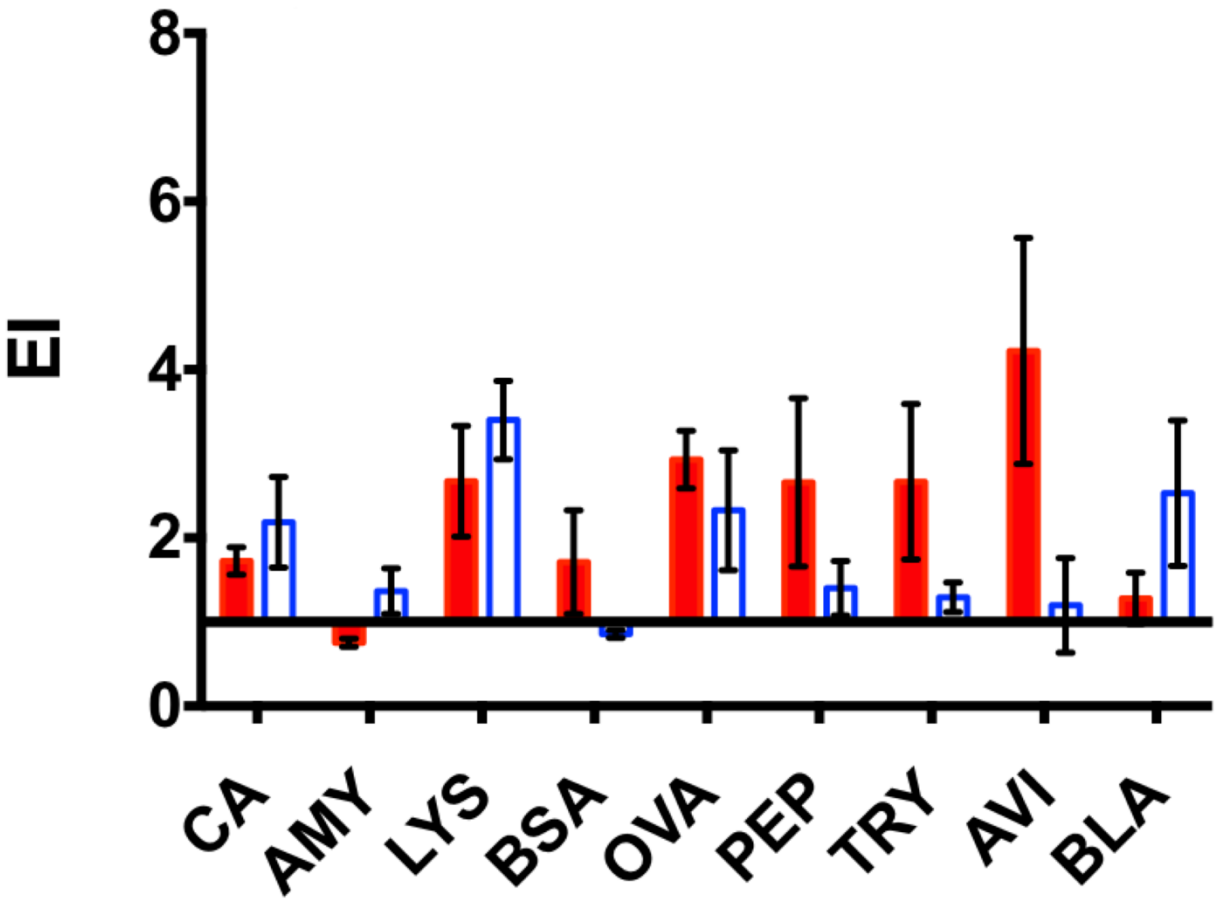


**Figure 5.** Enrichment Index (EI) of FITC-labeled proteins towards SHS particles. EI values were determined from CLSM images. The EI values were calculated as the ratio of the fluorescence inside and outside of the SHS particles. The protein concentration used for the CLSM measurements was 80 μM. The EI values were computed based on data collected from two separate (n = 2) microscopy experiments conducted for each complex. The error bars were calculated from the average of at least 4 SHS particles. The concentrations of the solutions for

**SHS1** and **SHS2** was 299 μM of G-derivative **1** or **2**, in 52 mM KSCN, PBS pH 7.4. All samples were incubated for 1 hour with or without protein, and imaging was performed via excitation with the 488 nm laser. Owing to the inherent variability in each sample, the total number of particles considered in the EI calculations ranged from as few as 4 particles to as many as 15, with an average of 6 particles. Refer to Table S4 for a detailed breakdown of the total particle counts used in these measurements.

The EI values for the tested proteins do not seem to have a strong correlation with the size of the SHS particle, which contrasts with the behavior observed for small molecule dyes.[16] For instance, the EI values for small molecule dyes towards **SHS1** generally fall within the range of 4 to 20, while for the same **SHS1** particle, most of the EI values for proteins range from 1 to 4.[2423]

The proteins' low apparent affinity towards the SHS particles in their natural state suggests the potential to develop methods to modify their affinity towards specific macromolecules. One such method could involve incorporating an affinity ligand to the SHS particles, which would allow for modulation of the affinity based on the system's properties. The G-derivatives of the SHS particles can be modified with a ligand to increase the affinity towards a target protein, as described in the following section.

*3.7 Modulation of protein affinity via heteromeric SHS particles*

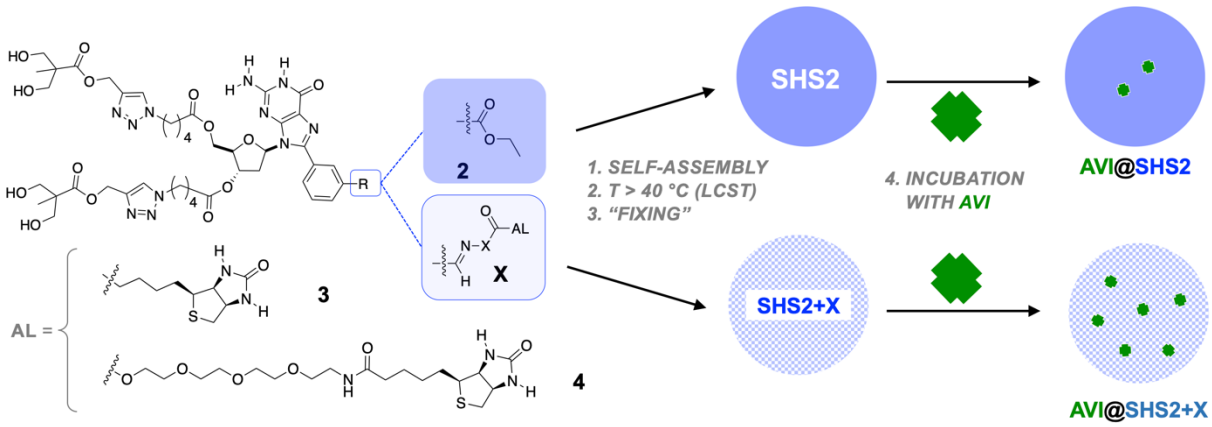


**Figure 6.** Experimental overview of the encapsulation methodology of proteins in SHS particles. (A) G-derivatives assembled isothermally (step 1) in the presence on a cation to form

supramolecular G-quadruplexes (SGQs) and the resulting SGQs are triggered to further assemble by increasing the temperature above the LCST (40 °C) (step 2), to from SHS microparticles, which are then kinetically stabilized ("fixed") by decreasing the ionic strength of the solution (step 3). Subsequent incubation with the desired protein (step 4: with AVI at 40 °C for 1 h) using either homomeric (**SHS2**) or heteromeric (**SHS2+X**) particles was finally analyzed via FC and/or CLSM as described in the text.

We selected **AVI** for our affinity modulation experiments because of its well-known high-affinity interaction with biotin. This interaction has been used for various purposes, such as catalysis [26] and targeting applications in drug delivery. [27] Previous studies have demonstrated that the surface of polymeric particles can be modified with biotin to encapsulate **AVI** or its analogues using "Click" reactions [28] or hydrazone formation. [29] However, incorporating affinity ligands directly onto the surface of a particle typically requires extensive purification efforts.[30] Instead, our approach involves modifying the G-derivative so that, when the corresponding SHS particle is formed, it results in a biotinylated colloid with potentially tunable affinity to **AVI** (Figure 6).We selected **AVI** for our affinity modulation experiments because of its well-known high-affinity interaction with biotin. This interaction has been used for various purposes, such as catalysis [25] and targeting applications in drug delivery. [26] Previous studies have demonstrated that the surface of polymeric particles can be modified with biotin to encapsulate **AVI** or its analogues using "Click" reactions [27] or hydrazone formation. [28] However, incorporating affinity ligands directly onto the surface of a particle typically requires extensive purification efforts.[29] Instead, our approach involves modifying the G-derivative so that, when the corresponding SHS particle is formed, it results in a biotinylated colloid with potentially tunable affinity to **AVI** (Figure 6).

To incorporate a biotin moiety into our G-derivative, we chose hydrazone formation using formyl-containing G-derivative **5**. [17] Hydrazine and hydrazides have been widely utilized in various fields, including dynamic combinatorial chemistry, molecular switches, and bioorthogonal chemistry, for incorporating functional groups into molecules containing aldehydes and ketones.[31-32] We synthesized two biotinylated G-derivatives (**biGs**) in a single step by combining **5** with commercially available biotin hydrazides, resulting in compounds **3** and **4** in high yields (Figure S35). [30-31] We synthesized two

biotinylated G-derivatives (**biGs**) in a single step by combining **5** with commercially available biotin hydrazides, resulting in compounds **3** and **4** in high yields (Figure S35). The difference between the two biotin-containing hydrazides is the presence of a longer "PEGylated" spacer with four ethylene oxide units separating the biotin moiety from the hydrazide group in derivative **4**. The acyl hydrazones **3** and **4** exist exclusively as the E isomer, but as a mixture of rotamers around the amide bond (NMR studies confirmed this; see Supporting Information for details; Figure S44), which did not affect the subsequent NMR self-assembly studies.

Earlier, we established that assembling G-derivatives is a crucial step in creating SHS particles.[10,33] Previous studies have also shown that by combining two types of G-derivatives, heteromeric SGQs can be formed, resulting in responsive properties that can be modulated.[33] Building on this, we hypothesized that using varying proportions of **2** with one of the biG derivative would enable us to adjust the apparent affinity of the resulting SHS particle towards **AVI**.Earlier, we established that assembling G-derivatives is a crucial step in creating SHS particles.[10,32] Previous studies have also shown that by combining two types of G-derivatives, heteromeric SGQs can be formed, resulting in responsive properties that can be modulated.[32] Building on this, we hypothesized that using varying proportions of **2** with one of the biG derivative would enable us to adjust the apparent affinity of the resulting SHS particle towards **AVI**.

We have reported that G-derivatives containing a meta-phenyl carbonyl group attached to the C8 of the guanine moiety form SGQs containing 16 subunits or hexadecamers.[19,34] Therefore, we anticipated that combining G-derivative **2** with biG-derivatives **3** or **4** would also lead to the formation of analogous hexadecameric SGQs. We have reported that G-derivatives containing a meta-phenyl carbonyl group attached to the C8 of the guanine moiety form SGQs containing 16 subunits or hexadecamers.[33,34] Therefore, we anticipated that combining G-derivative **2** with biG-derivatives **3** or **4** would also lead to the formation of analogous hexadecameric SGQs. The corresponding heteromeric assemblies, prepared by mixing G-derivatives **2** with biGs **3** or **4** in a ratio of 15:1 and 1:1, showed the characteristic double set of peaks found in the $^{1}$H NMR of hexadecameric SGQs like the homomeric **SGQ2**. This is particularly evident by inspecting the signature N1H region of 13-11 ppm (Figure S45B).

However, as anticipated, the spectra of the heteromeric **SGQ2+3** and **SGQ2+4** are more complex, due to their loss of symmetry, which includes the presence of assemblies containing different distributions of **3** or **4** within the SGQs, which is further complicated by the presence of various amide rotamers.

The molecular models depicted in Figure 7 (see Figure S52 for additional molecular model representations) offer insights into various aspects of the heteromeric SGQs. One aspect concerns the position of the biotin moiety within the assembly. Modifications to the biotin groups are expected to affect their accessibility to the binding pocket of the **AVI** subunits, potentially resulting in suboptimal interactions. [35] The models suggest that assemblies made with monomer **3** have the biotin moiety located near the solvent-exposed surface of the corresponding SGQ. This positioning is likely to affect the binding of **AVI** and, subsequently, the ability to modulate the properties of the resulting SHS particles. Conversely, assemblies containing derivative **4**, which feature a longer linker separating the biotin from the G-derivative, should induce lower steric hindrance between the SGQ and **AVI**, leading to correspondingly higher affinities. With these observations in mind, we assessed the apparent association constants using our FC protocol.

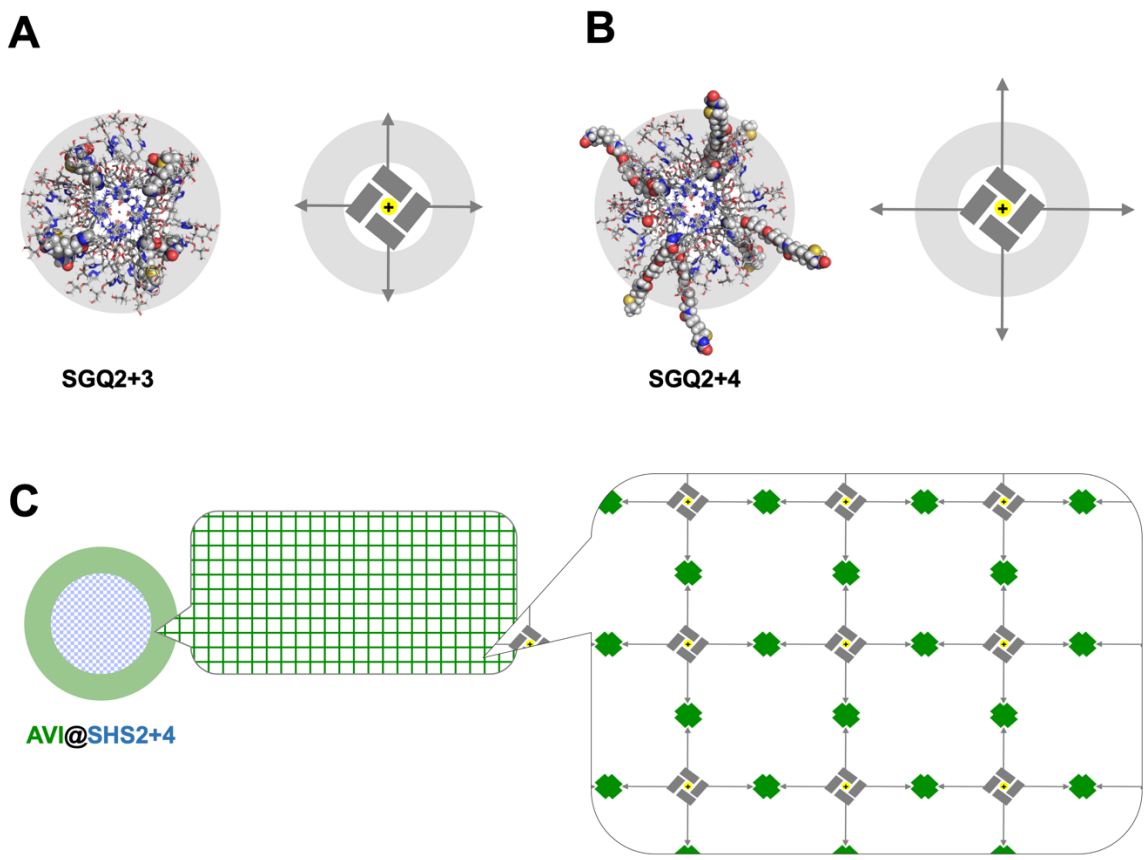


**Figure 7.** Linker length effect on biotin moiety availability in SGQ assemblies. Molecular models (right) of (A) **SGQ2+3** (1:1) and (B) **SGQ2+4** (1:1) and their corresponding schematic depictions (left). The SGQs are shown from a perspective looking down the central C4 axis (see Figure S52) with the region occupied by the ester chains highlighted with a light grey ring. The space-filling representations highlight the biotin moiety in the assembly (represented by arrows in the schematic depictions). (C) The longer linker in **SGQ2+4** (1:1), when combined with **AVI** (green figures), leads to a network structure that prevents further diffusion throughout the interior of the particle, thus **AVI** is concentrated on the periphery of the particle as determined by CLSM (Figure 9A). In contrast, the shorter linker in **SGQ2+3** (1:1) precludes these networks (possibly due to repulsive steric interactions) and prevents the formation of such networks, allowing a homogeneous distribution throughout the particle. For clarity purposes, the schematic depictions are simplified by showing a single tetramer made of the biotinylated derivative where the yellow circles with a + sign represent the potassium cations used to promote the formation of SGQs. Molecular models were generated and optimized using OPLS_2005 (MacroModel), version Maestro 9.3.5; Schrödinger, LLC: New York, 2007, with water as a continuous solvent.

To determine the affinity of the heteromeric SHS particles, we first measured their size and zeta potential (ZP) (Figure S46; Table S4). As expected, the heteromeric particles were larger than 1 μm in size, like their homomeric counterparts. However, the ZP

profiles of the heteromeric particles were significantly different from those of the homomeric particles. The addition of the biotin moiety led to more neutral ZP values for the heteromeric particles except for **SHS2+4** (1:1). For instance, **SHS2** had a ZP of (-9.0 ± 0.6) mV, whereas **SHS2+4** (15:1) had a ZP of (-1 ± 2) mV, and **SHS2+4** (1:1) had a ZP of (-4 ± 1) mV. The resulting colloidal suspensions are less stable than those of their homomeric counterparts, which increases the probability of subsequent aggregation.[36,37] Increasing the concentration seems to stabilize the particles, as seen with **SHS2+4** (1:1), which had the highest salt concentration and ZP among the particles reported in this study. While the ZP may have little or no adverse effect on protein affinity, it provides an interesting observation highlighting the consequences of incorporating biotin groups into these particles.

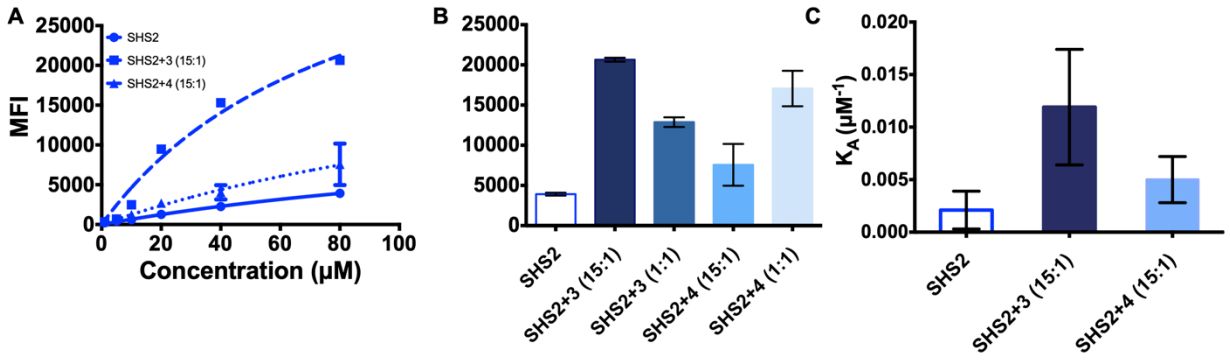


**Figure 8.** Binding isotherms, median fluorescence intensity (MFI) and the corresponding apparent association constants for the encapsulation of **FITC-AVI** in SHS particles for (A) **SHS2 SHS2+3** and **SHS2+4.** Error bars represent an average of 3 measurements. (B) MFI of the encapsulation of FITC-AVI (80 μM) and (C) apparent association constants ($K_A$) of FITC-labeled proteins towards **SHS2, SHS2+3** and **SHS2+4** determined from FC measurements. Error bars represent the standard error of the measurement reported by PRISM GraphPad. Conditions: All solutions were prepared in PBS 7.4; **SHS2**: 299 μM, 52 mM KSCN. **SHS2+3 (15:1):** 281 μM of **2** and 18 μM of **3** and 121 mM of KSCN. **SHS2+3 (1:1)**: 150 μM of G-derivatives and 242 mM of KSCN. **SHS2+4 (15:1):** 281 μM of **2** and 18 μM of **4** and 121 mM of KSCN. **SHS2+4 (1:1)**: 150 μM of G-derivatives and 121 mM of KSCN. For more details, see Table S5.

We used FC to measure the apparent affinity of heteromeric SHS particles and found that the **SHS2+X** (15:1) particles, regardless of the specific biotin moiety used, had increased affinity (Figure 8; Table S5). Our hypothesis was that as the concentration of

biotin increased, there would be a corresponding increase in affinity towards **AVI**. The saturation graph for **SHS2+3** (15:1) showed an increase in encapsulation relative to **AVI@SHS2**. However, we were unable to calculate the apparent affinity constants for the **SHS2+X** (1:1) complexes as the particles did not reach saturation within the measured concentration range (0-80 μM). Nonetheless, when examining the FC data at a concentration of 80 μM, we observed an increase in encapsulation compared to the homomeric assembly.

The MFI data for the heteromeric SHS particles provide insights into their behavior. The particle **SHS2+3** (1:1) shows a decrease in protein encapsulation compared to **SHS2+3** (15:1), which contrasts with **SHS2+4** (15:1) and **SHS2+4** (1:1). The latter two show an increase in encapsulation of **AVI** due to the higher concentration of biotinylated G-derivative. These differences suggest that SGQs containing derivative **3** have a limited number of available biotin subunits for binding to **AVI** as illustrated in Figure 7A due to their relatively buried distribution. In contrast, the longer linker in derivative **4** separates the biotin moiety from the assembly (Figure 7B), which is expected to prevent detrimental interactions with **AVI**. This is evidenced by the increase in MFI observed in **SHS2+4** upon increasing the proportion of **4** (Figure 8). Having established that incorporating biotin affinity ligands into the SHS particles leads to an enhanced apparent affinity, we then evaluated the corresponding effect on the distribution of **AVI** via confocal microscopy studies.

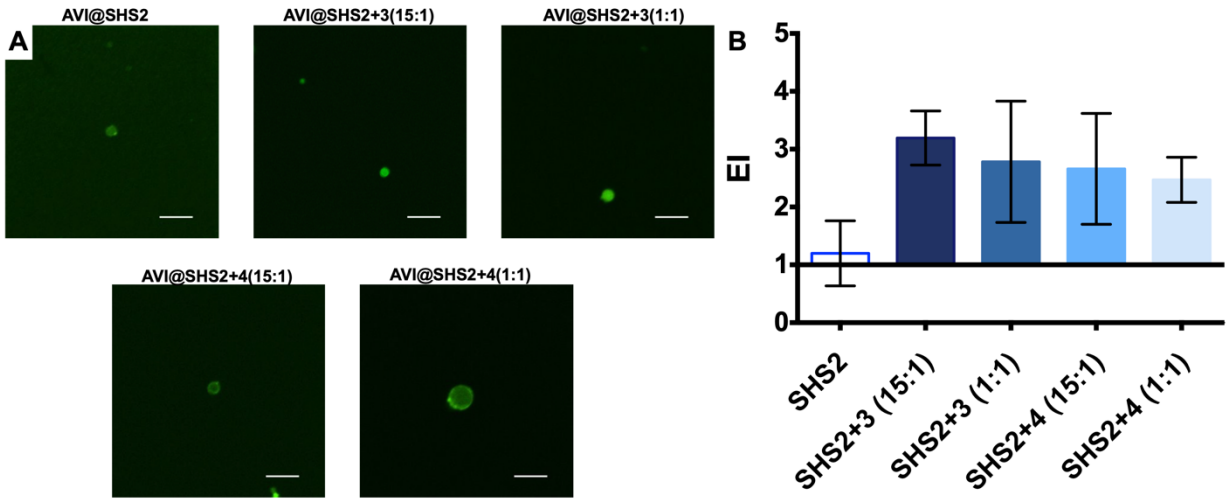


**Figure 9.** (A) Confocal microscopy images and (B) encapsulation efficiency (enrichment index) for **FITC-AVI** encapsulated (80 μM, excited at 488 nm) in homomeric and heteromeric SHS particles (Scale bar: 5 μm). The concentrations used were: **SHS2**: 299 μM, 52 mM KSCN, PBS pH 7.4. **SHS2+X (15:1):** 281 μM of **2** and 18 μM of **X**. **SHS2+X (1:1)**: 150 μM of G-derivatives where **X** = **3** or **4**. All heteromeric assemblies were prepared in PBS pH 7.4 and 121 mM KSCN, except **SHS2+4 (1:1)** that has a salt concentration of 242 mM of KSCN.

Figure 9 presents confocal microscopy images and an enrichment index graph of heteromeric SHS particles. The enrichment index of these proteins is lower compared to the encapsulation of small molecule dyes, even after adding the biotin ligand, suggesting the potential for improvement using this strategy.[16] The enrichment indexes of these particles demonstrate that incorporating the biotin ligand increases the affinity towards **AVI**. However, the nearly identical values of EI for all variants of **SHS2+3** and **SHS2+4** particles, as seen in the FC results, support the fact that the strong interaction between **AVI** and biotin results in irreversible interactions and similar saturation profiles. These images reveal different distributions of the encapsulated protein in **SHS2+3** and **SHS2+4** particles, with the former having a homogeneous distribution and the latter being concentrated in the periphery (peripheral encapsulation) (Figure 9). We hypothesize that the longer linker of the biotin moiety in **4** enables the formation of mesh networks on the outer layers of the SHS particles, preventing further diffusion of proteins deeper into the particles (see Figure 7C for a schematic depiction of this process). This suggests that future studies should focus on incorporating ligands with

lower affinity for the targeted protein to enable reversible interactions, maximizing interactions with the ligand throughout the entire particle.

## 4. CONCLUSIONS

In summary, this study underscores the effectiveness of our newly developed Flow Cytometry-based method for assessing protein complexation with colloidal particles, specifically focusing on SHS particles. While our method may not provide the precision necessary for determining absolute association constants (Ka values), it proves effective in establishing relative rankings among a set of proteins of interest. Furthermore, it offers a convenient way to quantify shifts in these apparent affinities when affinity ligands are introduced. To enhance the relatively low inherent affinity of proteins toward SHS particles, we devised a strategy involving the incorporation of biotinylated guanosine derivatives via hydrazone formation. While the results support this strategy for enhancing protein affinity, such enhancements were relatively modest. Analysis with confocal microscopy suggests saturation on the outer regions of SHS particles limited complete diffusion of **AVI** proteins throughout the particles. We anticipate that introducing lower-affinity ligands may lead to higher apparent affinities through multivalent effects, while still allowing reversible binding with the subsequent broad diffusion throughout the particles. Finally, although controlled release studies were not within the scope of this research, our results provide a promising step in that direction. Future efforts will focus on evaluating the release profile of encapsulated proteins in relation to ligand connectivity and incorporating triggering elements to finely control protein release profiles.

## Supporting Information

Supporting Information is available free of charge at https://pubs.acs.org

Preparative protocols, dynamic light scattering and Z-potential data, NMR spectra, flow cytometry data, histograms and density plots, saturation curves, CLSM images, and molecular models.


## Acknowledgments

We thank Jael A. Rodríguez Ortiz for his technical support and Dr. Valance Washington for generously lending us his group's Flow Cytometer. We also thank the Neuroimaging and Electrophysiology Facility, which is supported by a grant from NIH-NIGMS (P20GM103642), and Bismark A. Madera Soto, MS, MT, MLS (ASCP) CM for conducting the CLSM experiments at the Molecular Sciences Research Center. Finally, for fellowship support for LAPC and GRRC we also thank the RISE Program (5R25GM061151), while the MARC Program (5T34GM007821) provided support for JARO.

## References


(1) Farokhzad, O. C.; Langer, R. Impact of Nanotechnology on Drug Delivery. *ACS Nano* **2009**, *3* (1), 16–20. https://doi.org/10.1021/nn900002m.

(2) Bartus, R. T.; Tracy, M. A.; Emerich, D. F.; Zale, S. E. Sustained Delivery of Proteins for Novel Therapeutic Products. *Science* **1998**, *281* (5380), 1161–1162.

(3) Ye, C.; Chi, H. A Review of Recent Progress in Drug and Protein Encapsulation: Approaches, Applications and Challenges. *Mater. Sci. Eng. C* **2018**, *83*, 233–246. https://doi.org/10.1016/j.msec.2017.10.003.

(4) Lu, Y.; Sun, W.; Gu, Z. Stimuli-Responsive Nanomaterials for Therapeutic Protein Delivery. *J. Controlled Release* **2014**, *194*, 1–19. https://doi.org/10.1016/j.jconrel.2014.08.015.

(5) Wang, X.; Shi, C.; Zhang, L.; Bodman, A.; Guo, D.; Wang, L.; Hall, W. A.; Wilkens, S.; Luo, J. Affinity-Controlled Protein Encapsulation into Sub-30 Nm Telodendrimer Nanocarriers by Multivalent and Synergistic Interactions. *Biomaterials* **2016**, *101*, 258–271. https://doi.org/10.1016/j.biomaterials.2016.06.006.

(6) Pachioni-Vasconcelos, J. de A.; Lopes, A. M.; Apolinário, A. C.; Valenzuela-Oses, J. K.; Costa, J. S. R.; Nascimento, L. de O.; Pessoa, A.; Barbosa, L. R. S.; Rangel-Yagui, C. de O. Nanostructures for Protein Drug Delivery. *Biomater. Sci.* **2016**, *4* (2), 205–218. https://doi.org/10.1039/C5BM00360A.

(7) Vulic, K.; Shoichet, M. S. Affinity-Based Drug Delivery Systems for Tissue Repair and Regeneration. *Biomacromolecules* **2014**, *15* (11), 3867–3880. https://doi.org/10.1021/bm501084u.

(8) Wang, N. X.; von Recum, H. A. Affinity-Based Drug Delivery. *Macromol. Biosci.* **2011**, *11* (3), 321–332. https://doi.org/10.1002/mabi.201000206.

(9) Pakulska, M. M.; Miersch, S.; Shoichet, M. S. Designer Protein Delivery: From Natural to Engineered Affinity-Controlled Release Systems. *Science* **2016**, *351* (6279), aac4750–aac4750. https://doi.org/10.1126/science.aac4750.

(10) Betancourt, J. E.; Rivera, J. M. Nonpolymeric Thermosensitive Supramolecules. *J. Am. Chem. Soc.* **2009**, *131* (46), 16666–16668. https://doi.org/10.1021/ja9070927.

(11) Negrón, L. M.; Meléndez-Contés, Y.; Rivera, J. M. Patchy Supramolecules as Versatile Tools To Probe Hydrophobicity in Nanoglobular Systems. *J. Am. Chem. Soc.* **2013**, *135* (10), 3815–3817. https://doi.org/10.1021/ja401373h.

(12) Betancourt, J. E.; Subramani, C.; Serrano-Velez, J. L.; Rosa-Molinar, E.; Rotello, V. M.; Rivera, J. M. Drug Encapsulation within Self-Assembled Microglobules Formed by Thermoresponsive Supramolecules. *Chem. Commun.* **2010**, *46* (45), 8537. https://doi.org/10.1039/c0cc04063k.

(13) Negrón, L. M.; Díaz, T. L.; Ortiz-Quiles, E. O.; Dieppa-Matos, D.; Madera-Soto, B.; Rivera, J. M. Organic Nanoflowers from a Wide Variety of Molecules Templated by a Hierarchical Supramolecular Scaffold. *Langmuir* **2016**, *32* (10), 2283–2290. https://doi.org/10.1021/acs.langmuir.5b03946.

(14) Santos, S.; Ramírez, M.; Miranda, E.; Reyes, N.; Martínez, O.; Acosta-Santiago, M.; Rivera, J. M.; Otero, M. Enhancement of Immune Responses by Guanosine-Based Particles in DNA Plasmid Formulations against Infectious Diseases. *J. Immunol. Res.* **2019**, *2019*, 3409371. https://doi.org/10.1155/2019/3409371.

(15) Akamine, P.; González-Feliciano, J. A.; Almodóvar, R.; Morell, G.; Rivera, J.; Capó-Vélez, C. M.; Delgado-Vélez, M.; Prieto-Costas, L.; Madera, B.; Eichinger, D.; Pino, I.; Rivera, J. H.; Ortiz-Ubarri, J.; Rivera, J. M.; Baerga-Ortiz, A.; Lasalde-Dominicci, J. A. Optimizing the Production of Gp145, an HIV-1 Envelope Glycoprotein Vaccine Candidate and Its Encapsulation in Guanosine Microparticles. *Vaccines* **2023**, *11* (5), 975. https://doi.org/doi.org/10.3390/vaccines11050975.
(16) Prieto-Costas, L. A.; Milton, L.; Quiñones-Jurgensen, C. M.; Rivera, J. M. Screening and Quantification of the Encapsulation of Dyes in Supramolecular Particles. *Langmuir* **2021**, *37* (43), 12681–12689. https://doi.org/10.1021/acs.langmuir.1c02065.
(17) Acosta-Santiago, M. Biologically Relevant Formulation and Expansion of Responsive Properties of Guanine Based Supramolecular Particles. Ph.D., Universidad de Puerto Rico, San Juan, P.R., 2021.
(18) Rivera, J. M.; Negrón, L. M. Supramolecular Hacky Sacks (SHS), Method of Synthesis and Applications Thereof. 10106572, 2018.
(19) García-Arriaga, M.; Hobley, G.; Rivera, J. M. Structural Studies of Supramolecular G-Quadruplexes Formed from 8-Aryl-2′-Deoxyguanosine Derivatives. *J. Org. Chem.* **2016**, *81* (14), 6026–6035. https://doi.org/10.1021/acs.joc.6b01113.
(20) González-Rodríguez, D.; van Dongen, J. L. J.; Lutz, M.; Spek, A. L.; Schenning, A. P. H. J.; Meijer, E. W. G-Quadruplex Self-Assembly Regulated by Coulombic Interactions. *Nat. Chem.* **2009**, *1* (2), 151–155. https://doi.org/10.1038/nchem.177.
(21) Baldwin, R. L. How Hofmeister Ion Interactions Affect Protein Stability. *Biophys. J.* **1996**, *71* (4), 2056–2063. https://doi.org/10.1016/S0006-3495(96)79404-3.
(22) This Notation Is Inverted Relative to the One Previously Used by Us in Prior Publications,13,15 to Maintain Consistency with the Common Abbreviations for Host-Guest Complexes in Most Publications in the Field of Supramolecular Chemistry.
(23) Adan, A.; Alizada, G.; Kiraz, Y.; Baran, Y.; Nalbant, A. Flow Cytometry: Basic Principles and Applications. *Crit. Rev. Biotechnol.* **2017**, *37* (2), 163–176. https://doi.org/10.3109/07388551.2015.1128876.
(24) Schuster, B. S.; Reed, E. H.; Parthasarathy, R.; Jahnke, C. N.; Caldwell, R. M.; Bermudez, J. G.; Ramage, H.; Good, M. C.; Hammer, D. A. Controllable Protein Phase Separation and Modular Recruitment to Form Responsive Membraneless Organelles. *Nat. Commun.* **2018**, *9* (1), 2985. https://doi.org/10.1038/s41467-018-05403-1.
(25) Chen, C.; Zhu, S.; Huang, T.; Wang, S.; Yan, X. Analytical Techniques for Single-Liposome Characterization. *Anal. Methods* **2013**, *5* (9), 2150. https://doi.org/10.1039/c3ay40219c.
(26) Heinisch, T.; Ward, T. R. Artificial Metalloenzymes Based on the Biotin–Streptavidin Technology: Challenges and Opportunities. *Acc. Chem. Res.* **2016**, *49* (9), 1711–1721. https://doi.org/10.1021/acs.accounts.6b00235.
(27) Lee, E. S.; Na, K.; Bae, Y. H. Super PH-Sensitive Multifunctional Polymeric Micelle. *Nano Lett.* **2005**, *5* (2), 325–329. https://doi.org/10.1021/nl0479987.

(28) Wang, X.; Liu, L.; Luo, Y.; Zhao, H. Bioconjugation of Biotin to the Interfaces of Polymeric Micelles via In Situ Click Chemistry. *Langmuir* **2009**, *25* (2), 744–750. https://doi.org/10.1021/la802810w.
(29) Li, J.; Yang, S.; Wang, L.; Wang, X.; Liu, L. Thermoresponsive Dynamic Covalent Polymers with Tunable Properties. *Macromolecules* **2013**, *46* (17), 6832–6842. https://doi.org/10.1021/ma400948j.
(30) Ferreira Soares, D. C.; Oda, C. M. R.; Monteiro, L. O. F.; de Barros, A. L. B.; Tebaldi, M. L. Responsive Polymer Conjugates for Drug Delivery Applications: Recent Advances in Bioconjugation Methodologies. *J. Drug Target.* **2019**, *27* (4), 355–366. https://doi.org/10.1080/1061186X.2018.1499747.
(31) Skene, W. G.; Lehn, J.-M. P. Dynamers: Polyacylhydrazone Reversible Covalent Polymers, Component Exchange, and Constitutional Diversity. *Proc. Natl. Acad. Sci.* **2004**, *101* (22), 8270–8275. https://doi.org/10.1073/pnas.0401885101.
(32) Kölmel, D. K.; Kool, E. T. Oximes and Hydrazones in Bioconjugation: Mechanism and Catalysis. *Chem. Rev.* **2017**, *117* (15), 10358–10376. https://doi.org/10.1021/acs.chemrev.7b00090.
(33) Betancourt, J. E.; Rivera, J. M. Tuning Thermoresponsive Supramolecular G-Quadruplexes. *Langmuir* **2015**, *31* (7), 2095–2103. https://doi.org/10.1021/la504446k.
(34) García-Arriaga, M.; Acosta-Santiago, M.; Cruz, A.; Rivera-Rivera, J. M.; López, G. E.; Rivera, J. M. Probing the Limits of Supramolecular G-Quadruplexes Using Atomistic Molecular Dynamics Simulations. *Inorganica Chim. Acta* **2017**, *468*, 209–222. https://doi.org/10.1016/j.ica.2017.08.051.
(35) Terai, T.; Kohno, M.; Boncompain, G.; Sugiyama, S.; Saito, N.; Fujikake, R.; Ueno, T.; Komatsu, T.; Hanaoka, K.; Okabe, T.; Urano, Y.; Perez, F.; Nagano, T. Artificial Ligands of Streptavidin (ALiS): Discovery, Characterization, and Application for Reversible Control of Intracellular Protein Transport. *J. Am. Chem. Soc.* **2015**, *137* (33), 10464–10467. https://doi.org/10.1021/jacs.5b05672.
(36) To Avoid Aggregation, an Optimal ZP Is Estimated to Be within the Range of -30 MV to 30 MV (See Ref 36 for Details).
(37) Radomskasoukharev, A. Stability of Lipid Excipients in Solid Lipid Nanoparticles☆. *Adv. Drug Deliv. Rev.* **2007**, *59* (6), 411–418. https://doi.org/10.1016/j.addr.2007.04.004.

## TOC graphic